Geochemistry, Geophysics, Geosystems®

AGU ADVANCING EARTH AND SPACE SCIENCES

RESEARCH ARTICLE
10.1029/2024GC011748

Patterns of Plio-Pleistocene Ice Volume Variability Recorded by the Large-Magnitude Explosive Eruptions From the Kamchatka-Kurile Volcanic Arc

Susanne M. Straub[1], Brendan Reilly[1], Maureen E. Raymo[1], Arturo Gómez-Tuena[2], Kuo-Lung Wang[3,4], Elisabeth Widom[5], David Kuentz[5], and Richard J. Arculus[6]

[1]Lamont Doherty Earth Observatory at the Columbia University, Palisades, NY, USA, [2]Laboratorio Nacional de Geoquímica y Mineralogía, Instituto de Geología, Universidad Nacional Autónoma de México, Ciudad de México, Mexico, [3]Institute of Earth Sciences, Academia Sinica, Taipei, Taiwan, [4]Department of Geosciences, National Taiwan University, Taipei, Taiwan, [5]Department of Geology and Environmental Earth Science, Miami University, Oxford, OH, USA, [6]Research School of Earth Science, Australia National University, Canberra, ACT, Australia

Key Points:

- Marine fallout ash beds record cyclicity and acceleration of the Plio-Pleistocene (0–4 Myr) explosive Kamchatka-Kurile arc volcanism
- Ash bed cyclicity correlates with the obliquity and precession variance of the global ice volume
- Climate, and not direct orbital forcing, modulates the Plio-Pleistocene volcanicity of the Kamchatka-Kurile arc

Supporting Information:

Supporting Information may be found in the online version of this article.

Correspondence to:

S. M. Straub,
smstraub@ldeo.columbia.edu

Citation:

Straub, S. M., Reilly, B., Raymo, M. E., Gómez-Tuena, A., Wang, K.-L., Widom, E., et al. (2024). Patterns of Plio-Pleistocene ice volume variability recorded by the large-magnitude explosive eruptions from the Kamchatka-Kurile volcanic arc. *Geochemistry, Geophysics, Geosystems*, *25*, e2024GC011748. https://doi.org/10.1029/2024GC011748

Received 3 JUL 2024
Accepted 20 SEP 2024

Author Contributions:

Conceptualization: Susanne M. Straub, Brendan Reilly, Maureen E. Raymo
Formal analysis: Susanne M. Straub, Brendan Reilly, Arturo Gómez-Tuena, Kuo-Lung Wang, Elisabeth Widom, David Kuentz
Funding acquisition: Susanne M. Straub, Maureen E. Raymo, Richard J. Arculus
Investigation: Susanne M. Straub, Brendan Reilly
Methodology: Susanne M. Straub, Brendan Reilly

Abstract

Marine fallout ash beds can provide continuous, time-precise records of highly explosive arc volcanism that can be linked with the climate record. An evaluation of revised Plio-Pleistocene (0–4 Myr) tephrostratigraphies from Ocean Drilling Program Sites 881, 882, and 884 confirms cyclicity of the Kamchatka-Kurile arc volcanism and a marked increase just after the intensification of the Northern Hemisphere glaciation at 2.73 Ma. The compositional constancy of the Kamchatka-Kurile volcano-magma systems through time points to external modulation of volcanic cyclicity and frequency. The stacked tephra record reveals periodic peaks in arc volcanicity at ~0.3, ~1.0, ~1.6, ~2.5, and ~3.8 Myr that coincide with maxima of the global ice volume variability that have been linked with the amplitude modulation of the precession (0.3, 1.0 Myr) and obliquity (1.6, 2.5 and 3.8 Myr) bands. A simple model of a decreasing obliquity variance across the mid-Pleistocene Transition at constant precession variance produces an excellent correlation of ash bed cycles with the variability of global benthic $\delta^{18}O$ ($r^2 = 0.75$), which implies that climate, and not direct orbital forcing, modulates Kamchatka-Kurile arc volcanism. The rising influence of precession variance in the Kamchatka-Kurile ash bed record after the mid-Pleistocene Transition contrasts with the dominant 100 kyr signal in the benthic $\delta^{18}O$ global ice volume variability, which may either reflect limitations of the ash bed record or an regional rather than global influence of ice volume variability. Our results indicate that climate influences the Kamchatka-Kurile arc volcanism, which may influence climate only by feedback.

Plain Language Summary

Volcanic ash and dust produced during catastrophic explosive volcanic eruptions, such as those of Mount Pinatubo or El Chichón, can cause short-term global cooling on the scale of a few years. It has long been speculated whether the Earth's long-term cooling over the past few million years has been augmented by an increase in explosive volcanism about 2.58 million years ago. In order to investigate causal links between the climate evolution and volcanism during the past 4 million years, we obtained a time-precise and temporally highly resolved record of the Kamchatka-Kurile arc volcanism from the centimeter-thick ash beds that were embedded in marine sediments after large eruptions downwind the volcanic sources. When the ash bed record is compared to climate evolution, it clearly shows that explosive volcanic eruptions—regardless of their short-term effects—do not contribute directly to the long-term global cooling. Instead, the variations of the Earth's powerful climate system modulate these explosive volcanic eruptions, as the periodic waxing and waning of the large ice shields affect the magma-producing systems deep in the Earth's interior. However, climate-active gases and particles produced during periods with more vigorous arc volcanism may still enhance the ice cycles.

1. Introduction

There has been a long-standing discussion about causal links between volcanism and Plio-Pleistocene climate evolution (e.g., Huybers & Langmuir, 2009; Kennett & Thunell, 1977; Kutterolf et al., 2013). The debate started with the discovery of a marked increase in the frequency of marine fallout ash bed sediments at the Plio-Pleistocene boundary [=Matuyama-Gauss reversal] about ~2.58 million years ago in the wake of the Deep Sea Drilling Project (Kennett & Thunell, 1977). The increase in tephra bed frequency in the Pleistocene was subsequently confirmed as a robust global-scale feature by studies that utilized the improved core quality and

Project administration: Susanne M. Straub
Visualization: Susanne M. Straub, Brendan Reilly
Writing – original draft: Susanne M. Straub, Brendan Reilly
Writing – review & editing: Susanne M. Straub, Brendan Reilly, Maureen E. Raymo, Arturo Gómez-Tuena, Kuo-Lung Wang, Elisabeth Widom, David Kuentz, Richard J. Arculus

recovery of the Ocean Drilling Program (ODP), the Integrated ODP and the International Ocean Discovery Program (IODP) (e.g., Cambray et al., 1993; Mahony et al., 2016; Pank et al., 2023; Prueher & Rea, 1998; Straub & Schmincke, 1998). With improved core recovery, it also became evident that the Plio-Pleistocene ash bed record can display cyclic patterns that are independent of compositional variations that could link them to volcanic or tectonic evolution (Cao et al., 1995; Ponomareva et al., 2023; Schindlbeck, Jegen, et al., 2018; Schindlbeck, Kutterolf, et al., 2018). Because marine fallout ash beds document explosive volcanism over millions of years with far better resolution, precision and completeness than any subaerial record, several studies have tested ash bed time series for the presence of orbital-related cyclicities that modulate climate (Kutterolf et al., 2013, 2019; Kutterolf et al., 2019; Paterne et al., 1988; Schindlbeck, Jegen, et al., 2018; Zelenin et al., 2024). However, it became quickly evident that truly suitable tephrostratigraphies are difficult to obtain (e.g., Kutterolf et al., 2019; Mahony et al., 2016). Ideally, such tephrostratigraphies build on 100% recovery of datable sediment cores that are interspersed with abundant tephra beds. The sedimentation environment must have been reasonably stable to minimize syn- and post-depositional modification or destruction of ash beds (and host sediment) by bottom currents, erosion, faulting, slumping, and bioturbation (e.g., Bubenshchikova et al., 2024; Freundt et al., 2021). Preferably, the ash should originate from a single source region so as to eliminate magma-producing disparities among different arcs and to allow for estimating the eruptive magnitudes from known sources as well as covering several million years of climate evolution with a sufficient resolution. In reality, these conditions rarely converge. Current studies of marine tephra bed series are mostly limited to the last ∼1 to ∼1.1 million years (e.g., Kutterolf et al., 2019; Longman et al., 2024; Schindlbeck, Jegen, et al., 2018). However, only one study from a single drill hole gave a clear 100 kyr orbital signal (Schindlbeck, Jegen, et al., 2018). A single study encompassing the last 6 million years failed to discover orbital-scale cyclicities (Zelenin et al., 2024). There are also limitations due to inherent uncertainties of the data compilation, where the sheer mass of the data commonly prohibits screening of individual ash beds for misidentification or provenance and forces the use of preliminary shipboard age models (Kutterolf et al., 2013; Mahony et al., 2020; Straub & Schmincke, 1998). These problems perpetuate through the subsequent statistical analyses of tephra bed time series (Kutterolf et al., 2013, 2019; Longman et al., 2024). While there are indications of cyclicities, the analyses remain tantalizingly inconclusive with respect to a potential climate connection and its causes. To overcome these problems, we searched for datable, complete tephrostratigraphies that cover the entire Plio- to Pleistocene global cooling trend, and found them at ODP Sites 881, 882, and 884 in the northwest Pacific Ocean.

2. Geological Setting and Samples: The Ash Bed Record

ODP Sites 882 and 884 are located on the Detroit Seamount at the northern Emperor Seamount Chain. Site 882 (50.35°N 167.58°E) was drilled in 3,244 m water depth on a plateau of the southern Detroit Seamount (Rea et al., 1993). Site 884 (51.45°N, 168.33°E) was drilled ∼133 km to the northeast of Site 882 in 3,825 m water depth on the northeast flank of the Detroit seamount. Site 881 (47.10°N, 61.48°E) was drilled ∼575 km to the southwest of Site 882 (Figure 1) in 5,531 m water depth on the abyssal plain. The sediments are a mixture of non-calcareous biogenic (clayey diatom ooze, diatom ooze, radiolarian/diatom ooze) and terrigenous components, the latter comprising eolian dust, volcanic ash and ice-rafted debris (IRD). After ∼2.75 Ma, the biogenic component decreased, while the terrigenous flux increased and discrete (macroscopically visible) ash beds became more frequent (e.g., Bailey et al., 2011; Rea et al., 1993). Discrete volcanic ash beds, while frequent, contribute only ∼2% to the total sediment thickness.

The volcanic ash beds at Sites 881–884 have been described in detail by Rea et al. (1993), Cao et al. (1995), and Ponomareva et al. (2023). Thus, only a few salient points are summarized here. The volcanic ash is mostly concentrated in centimeter-thick and sometimes decimeter-thick layers, and occasionally in centimeter -sized ash pods and burrows (Figures S1 and S2, https://doi.org/10.60520/IEDA/113223). Most of the ash is light-colored. Thinner (<1 cm) beds of light-colored ash are very rare, presumably because they are destroyed by the pervasive bioturbation, which visibly disintegrates ash beds and can create intervals with dispersed, mm-sized streaks and pods of light-colored ash. The rarer dark ash beds are usually thinner, and seem more resistant to bioturbation. Fully formed ash beds exhibit the typical characteristics of fallout emplacement of airborne ash from explosive eruptions, which include sharp bases, normal grading and a transitional top. Fallout origin is consistent with the prevalence of well-sorted, colorless glass shards that include sharply pointed bubble wall glass fragments to pumiceous and round and tubular glass fragments. Typical accessory phases are plagioclase, and rarely pyroxene, Fe-Ti oxides, biotite, and amphibole (Cao et al., 1995; Ponomareva et al., 2023; Rea et al., 1993). The tephra is

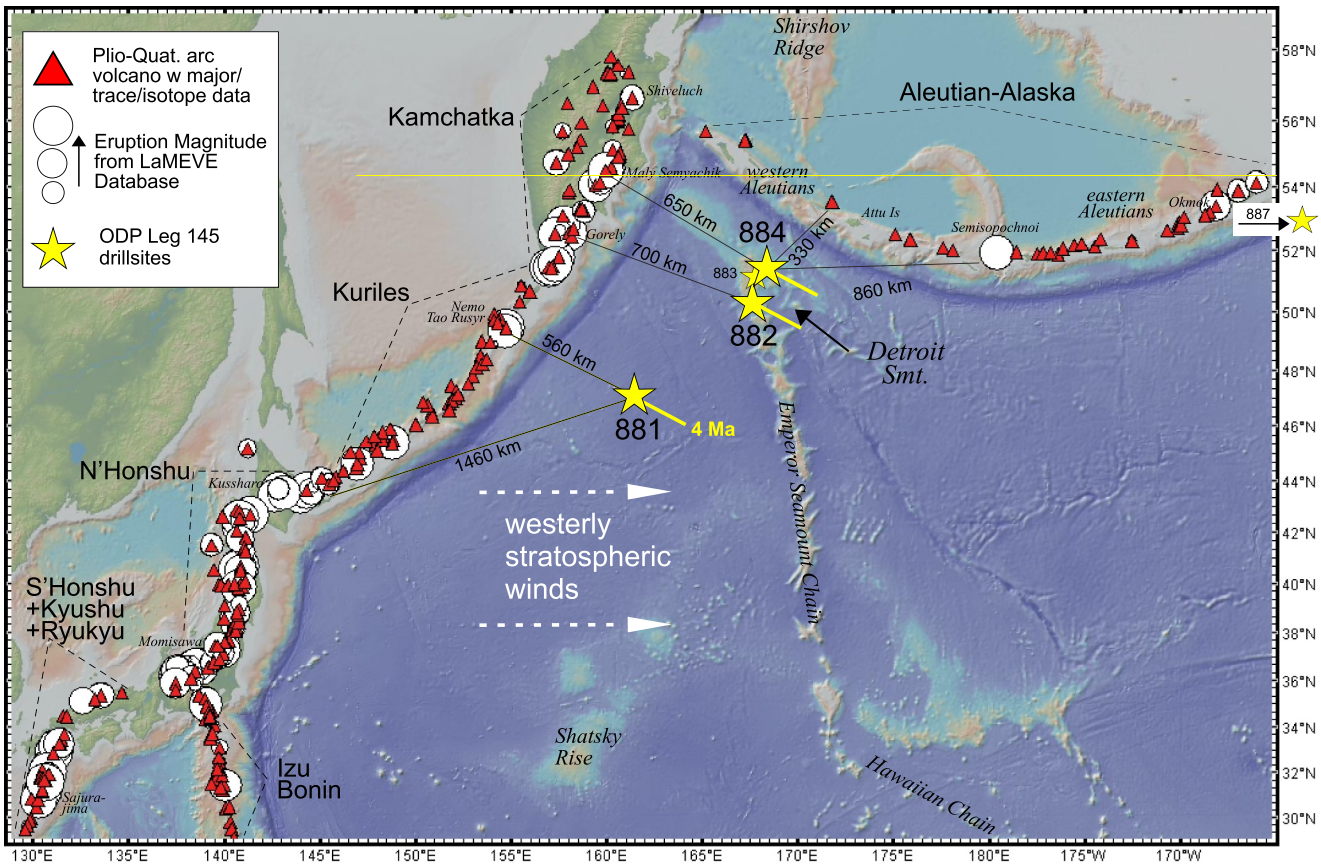

Figure 1. Northwestern Pacific volcanic arcs in relation to Leg 145 drill sites. All arc volcanoes (red triangles) shown have geochemical data (Straub, 2017). Eruptive magnitudes (white circles) are from the LaMEVE database (Crosweller et al., 2012). *Thick yellow lines*—indicate plate movement of site for 4 Ma (~300–330 km). *Stippled white lines*—prevailing stratospheric wind direction for the entire north Pacific.

exclusively ash-sized (<2,000 μm), except for very rare pumice lapilli that are unrelated to the ash beds, and likely dropped from a pumice raft or an iceberg (Ponomareva et al., 2023; Rea et al., 1993) and that do not represent a single explosive volcanic event.

3. Tephrostratigraphies of Site 881, 882, and 884

Site 881–884 sediments are well-dated despite being deposited below the Plio-Pleistocene calcite compensation depth. Sediment ages were obtained from high-quality magnetostratigraphy, which is supported by diatom and radiolaria biostratigraphy (Barron et al., 1995). Ponomareva et al. (2023) refined sediment ages for Hole 882A and Hole 884B through a revision of published magnetostratigraphic ages (Rea et al., 1993; Weeks et al., 1995), and correlation with the <1.1 Myr ash bed record of a 45 m giant piston core (MD01-2416) that was taken between Sites 882 and 884 in shallower water depth of 2,317 mbsl, and which was dated by a combination of magneto- and $\delta^{18}O$ stratigraphy. While the stratigraphies of Holes 882A and 884B are solid, they still have coring gaps of up to several meters in length (Rea et al., 1993). Coring gaps, however, are eliminated for a splice of Holes 882A and 882B ("Site 882AB-splice"), for which an astronomically calibrated stratigraphy was manufactured based on magnetostratigraphy and fine tuning of GRAPE (gamma ray attenuation porosity evaluator) density oscillations in the orbital precession band to the summer insolation at 65°N (Tiedemann & Haug, 1995). The tuned stratigraphy compares within an error limit of a few thousand years to other tuned paleo-oceanographic and climate records, and arguably presents a complete sediment record free from hiati and coring gaps until 4.16 Ma (297.13 mbsf).

A primary target of this study was to build a complete, 0–4 Ma tephrostratigraphy, "882AB-splice." The "882AB-splice" was complemented by a revised tephrostratigraphy of Site 881, which was built from Holes 881B and

Table 1
Summary of Hole Used for Time Series 0–4.21 Ma

			No. ash beds ≤4.3 Ma	No ash beds per Ma
882AB splice	Tiedemann and Haug (1995)	Astronomical[a]	75	18
882AB splice	Tiedemann and Haug (1995)	Paleomagnetics[b]	77	18
Hole 882A	Ponomareva et al. (2023)	Ash bed correlation (<1.1 Ma); paleomagnetics	60	14
Hole 884B	Ponomareva et al. (2023)	Ash bed correlation (<1.1 Ma); paleomagnetics	58	13
Hole 881B/D	Barron et al. (1995)	Paleomagnetics	147	37

[a]Astronomical time scale of Tiedemann and Haug (1995) ("882 cycle ages"). [b]Paleomagnetic time scale of Tiedemann and Haug (1995) ("882 pmag ages").

881D, and which provides the longest Pleistocene record closest to the Kamchatka-Kurile arc (Figure 1). Together, the Site 881 and 882 tephrostratigraphies should represent the Plio-Pleistocene volcanism of the Kamchatka-Kurile arc. In addition, we included the recently published tephrostratigraphies of Hole 882A and Hole 884B (Ponomareva et al., 2023) in order to assess the robustness of the tephrostratigraphies and the existence of communal cyclicities. Detailed descriptions of the revised tephrostratigraphies are given in Text S2 in Supporting Information S1. The ash bed series of Sites 881–844 are summarized in Table 1.

4. Compositional Data of Site 881, 882, and 884 Ash Beds

Major and trace element compositions of Site 881, 882 and 884 glass shards and bulk tephra have been reported by Cao et al. (1995) and Ponomareva et al. (2023). Additionally, Cao et al. (1995) reported Sr-Nd isotope ratios of 19 bulk tephras from Sites 881 and 882. In this study, we report additional major and trace element glass shard data for the ash beds of the Site 882AB-splice in order to (a) assess the validity of the Site 882AB-splice through Hole A-B tephra bed correlation; (b) safely combine ash beds from both holes for having sufficient ash material for "bulk tephra" analyses (see Text S2 in Supporting Information S1), and (c) provide a complete compositional profile for the last 4 Ma. Because glass shards of some tephra beds were too small for laser-ablation ICP-MS analysis, we obtained trace elements by solution ICP-MS from separated fresh volcanic particles (glass shards, scoria = "bulk tephra," see Text S2 in Supporting Information S1) of 17 ash beds. We also report Pb-Nd isotope ratios for 50 "bulk tephra" samples of the Site 882AB-splice for their potential to verify ash provenance and assess temporal variations. The details of preparation and analytical methods are given in Text S2 in Supporting Information S1. All analytical data are compiled in Tables S3–S6, https://doi.org/10.60520/IEDA/113223.

5. Results: Constraints From Ash Bed Composition and Thickness

Ash bed composition and thickness provide key insights into ash provenance, eruptive magnitude and temporal evolution of the ash-producing magmatic systems of the Site 881–884 Plio-Pleistocene tephrostratigraphies that form the basis for evaluating a climate signal.

5.1. Tephra Provenance From the Kamchatka-Kurile Arc

Characteristic major and trace element variations of the Site 881–884 ash beds clearly identify them as arc-derived (Cao et al., 1995; Ponomareva et al., 2023, this study). Moreover, land-sea correlation studies confirmed ash provenance from the Kamchatka-Kurile arc for many ash beds younger than 450 ka (Cao et al., 1995; Ponomareva et al., 2018, 2023). Here, the new Pb isotope data for the Site 882AB splice confirm for the first time that the Kamchatka-Kurile arc is the dominant source of the ash since at least 3.9 Ma (Figure 2), as all 50 ashes analyzed have the characteristic Pb isotope ratios of the Kamchatka-Kurile arc. This includes all thicker, rhyolitic ash beds for which sufficient material for isotope analysis was easily obtained, as well as many of the thinner, dark-colored andesitic ash beds. Most ash beds can be linked to the Kamchatka segment; only a few tephra beds have the higher $^{206}Pb/^{204}Pb$ (>18.40) suggestive of a Kurile arc origin. To date, there is no confirmed input from the Aleutian and Honshu arcs, even if such origin cannot be ruled out with certainty for thin and/or poorly formed tephra beds for which no Pb isotope data could be obtained.

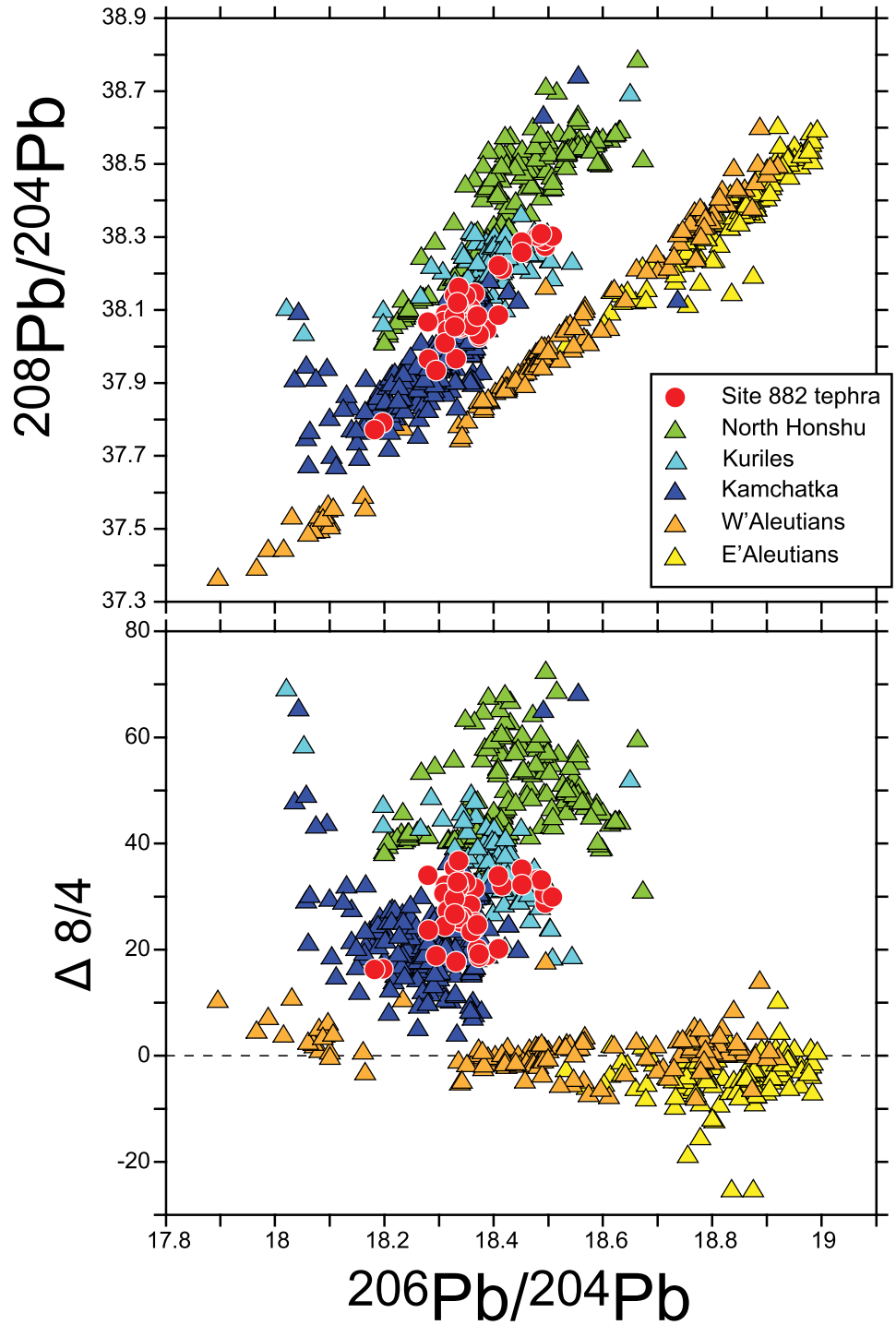

Figure 2. (a) $^{206}Pb/^{204}Pb$ versus $^{208}Pb/^{204}Pb$, and (b) $^{206}Pb/^{204}Pb$ versus Δ8/4, where Δ8/4 = [($^{208}Pb/^{204}Pb$) − (1.209 × $^{206}Pb/^{204}Pb$ + 15.6270)] (Dupre & Allegre, 1983) is a measure of mantle source enrichment, which distinguishes the Kamchatka-Kurile from the Aleutians and Honshu arc. Western versus Eastern Aleutians separated at 170°W. Arc compositional data from Straub (2017).

A Kamchatka-Kurile origin for the Site 882 ash beds implies a similar origin for ash beds at Sites 881 and 884, which lie in the same zone of prevailing westerly winds. Thirty-four ash beds with ages between 42 ka and 3.8 Ma can be correlated between Sites 882 and 884 (Ponomareva et al., 2023); 21 of these 34 ash beds have Kamchatka-

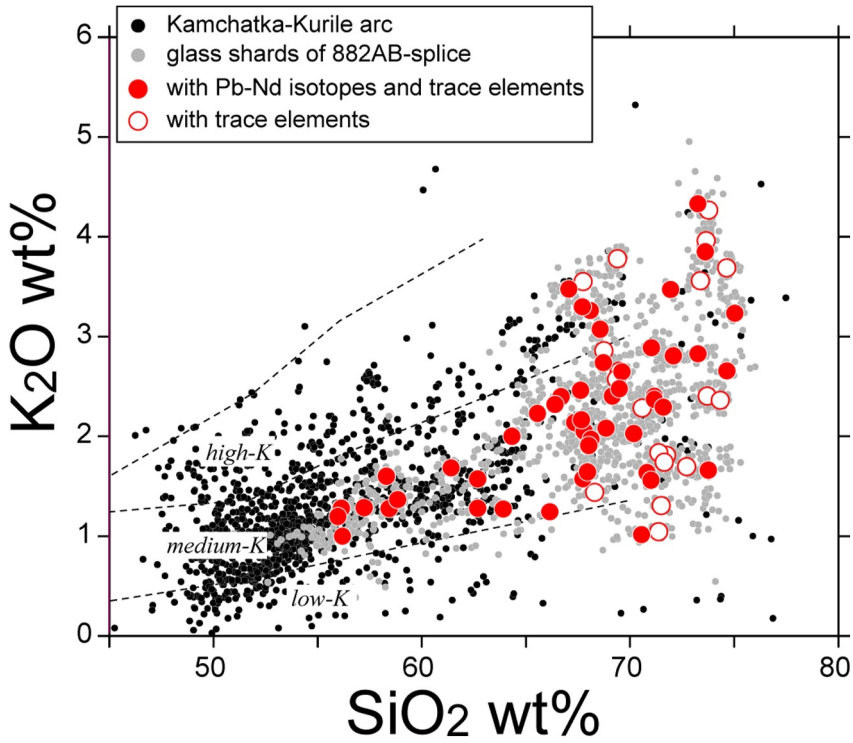

Figure 3. K_2O wt% versus SiO_2 wt% of glass shards (gray) from the Site 882AB-splice compared to Kamchatka-Kurile arc volcanic rocks (Straub, 2017). Filled red circles mark the 50 (out of the 77) "bulk tephras" analyzed for Pb-Nd isotopes and trace elements. Open red circles denote ash beds for which only trace element data have been obtained. Sites 881 and 884 glass shards display the same range in the K_2O versus SiO_2 space (Cao et al., 1995; Ponomareva et al., 2023) but are not plotted for clarity.

Kurile-type Pb isotope data. No Pb isotope data exist for Site 881 ash beds, but that Site is closest to the Kamchatka-Kurile arc. Site 881 may receive more Kurile than Kamchatka ash, even if the thickest ash bed, the 55 cm thick Pauzhetka ash at ~423 ka, originates from southern Kamchatka (Ponomareva et al., 2018).

The Pb-Nd isotope ratios and trace element data show that the typical spectrum of low-K to high-K melts produced in the Kamchatka-Kurile arc is well represented by the distal ash beds, even if the ash is more silicic than the mafic lavas in the source area (Figure 3).

5.2. A Cyclic Record of Large Magnitude Explosive Eruptions

It is well-known that only large explosive eruptions with eruption magnitudes of $M_v \geq 5$ form marine ash beds (e.g., Kutterolf et al., 2018; Mahony et al., 2016; Schindlbeck, Kutterolf, et al., 2018). Minimum eruption magnitudes of marine ash beds from single holes are usually calculated after Legros (2000) and Pyle (1995) as a function of ash bed thickness, distance to source, and an assumed (minimum) dispersal area (see Text S2 in Supporting Information S1 for calculation of M_v). Unsurprisingly, minimum eruption magnitudes of M_v ~5 to ~7 are obtained for all Site 881–884 ash beds (Figure 4, Ponomareva et al., 2023, this study). The calculation includes a correction for the distance to source and plate movement toward the Kamchatka-Kurile arc, and thus smooths out differences in ash bed thickness, which decrease with increasing distance to source. Similar M_v's are calculated for each site, suggesting that the Site 881–884 ash beds record only cataclysmic, large-magnitude eruptions of the Kamchatka-Kurile arc, which compare in size to the historic eruptions of Vesuvius 79 ($M_v = 5$), Pinatubo 1991 ($M_v = 6$) or Mt. Tambora 1815 ($M_v = 7$).

The fact that eruptions with M_v ~5 to 7 form the Site 881–884 ash bed record does not imply the absence of smaller eruptions with $M_v < 5$, which are typically far more frequent than the larger eruptions given the inverse correlation of the eruption magnitude and frequency (Deligne et al., 2010; Mason et al., 2004). This simply means that the smaller eruptions do not produce sufficient ash flux to form discrete marine tephra beds, and that ash

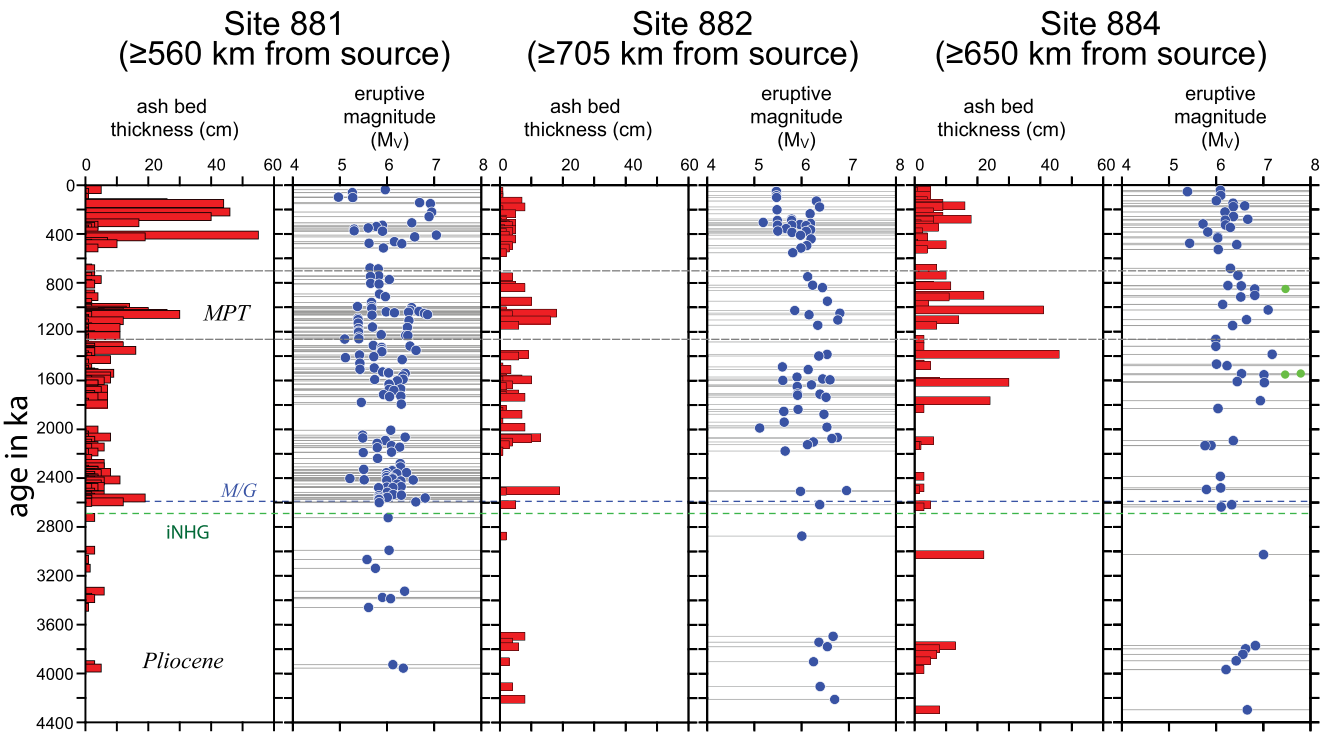

Figure 4. Ash bed thickness and calculated eruptive magnitude (M_v) versus time for Ocean Drilling Program Sites 881, 882, and 884. See Text S2 in Supporting Information S1 for calculation eruptive magnitude (M_v). Ash bed thicknesses at Site 884 may be somewhat compromised by post-depositional thickening, ocean bottom currents (Ponomareva et al., 2023), or drilling disturbance and lower core recovery >1600 years. MPT—Mid-Pleistocene Transition; M/G—Matuyama/Gauss reversal at 2.58 Ma; iNHG—intensification of the Northern Hemisphere Glaciation at 2.73 Ma. Green dots denote the tephra layer of Site 884, which was likely artificially thickened by ocean currents (Ponomareva et al., 2023), and for which M_v was calculated with corrected thickness (see Text S2 in Supporting Information S1).

instead accumulates as an invisible, cryptic component in the sediment. It is also possible that the Site 881–884 ash bed record hides super-eruptions with $M_v \geq 8$ which can impact the global climate for decades (e.g., Brenna et al., 2020). However, super-eruptions are rare (on the order of 4–22 events per million year worldwide, Mason et al., 2004) and they can only be identified from a larger number of well-distributed cores. The largest eruption thus far identified (the Pauzhetka eruption of southern Kamchatka at ~423 ka) has an eruption magnitude of ~7.60–7.65 and was found at all three drill sites (Ponomareva et al., 2018, 2023).

The minimum M_v calculated lacks any unidirectional trends with time (Figure 4). However, at all sites, there are peaks in ash count and thickness at ~0.2 to 0.4 Ma, at ~1–1.2 Myr during the MPT, and also prior to the MPT, where the ash record of the more distant Sites 882 and 884 may be less complete during the larger distance to source. These peaks are not carved out by variations in the sedimentation rate, which overall decreases at Sites 882 and 884, but increases at Site 881 in the Pleistocene. An effect of plate movement can also be ruled out, as the ash bed count and thickness at Site 881–884 show parallel fluctuations despite their different distances to source (Figure 1). Overall, these observations indicate that the explosive M_v ~5 to ~7 eruptions become periodically larger and more frequent, which supports observations of Pleistocene cyclicity of the ash bed count made previously by Cao et al. (1995) and Ponomareva et al. (2023).

5.3. Temporal Constancy of the Kamchatka-Kurile Arc Volcanism

An important result is that the ash bed composition and thickness provide no evidence for a temporal change in the Kamchatka-Kurile arc explosive volcanism. The compositional constancy is illustrated by selected variables for the 882AB-splice for which the data set is most complete (Figures 5 and 6). The SiO_2, K_{70} and Cl_{70} (K_2O and Cl normalized to a SiO_2 value of 70 wt%) (from glass shards), and $^{206}Pb/^{204}Pb$, $^{143}Nd/^{144}Nd$, Nd/La and Nd/Pb ratios (from "bulk tephra") are sensitive to mantle source composition but also to crustal processing (e.g., Bryant et al., 1999; Bryant et al., 2003; Straub, 2003; Straub et al., 2015). $^{206}Pb/^{204}Pb$ and $^{143}Nd/^{144}Nd$, which can only be changed by melt mixing, are entirely within the range of Kamchatka-Kuriles volcanic rocks (Straub, 2017), and

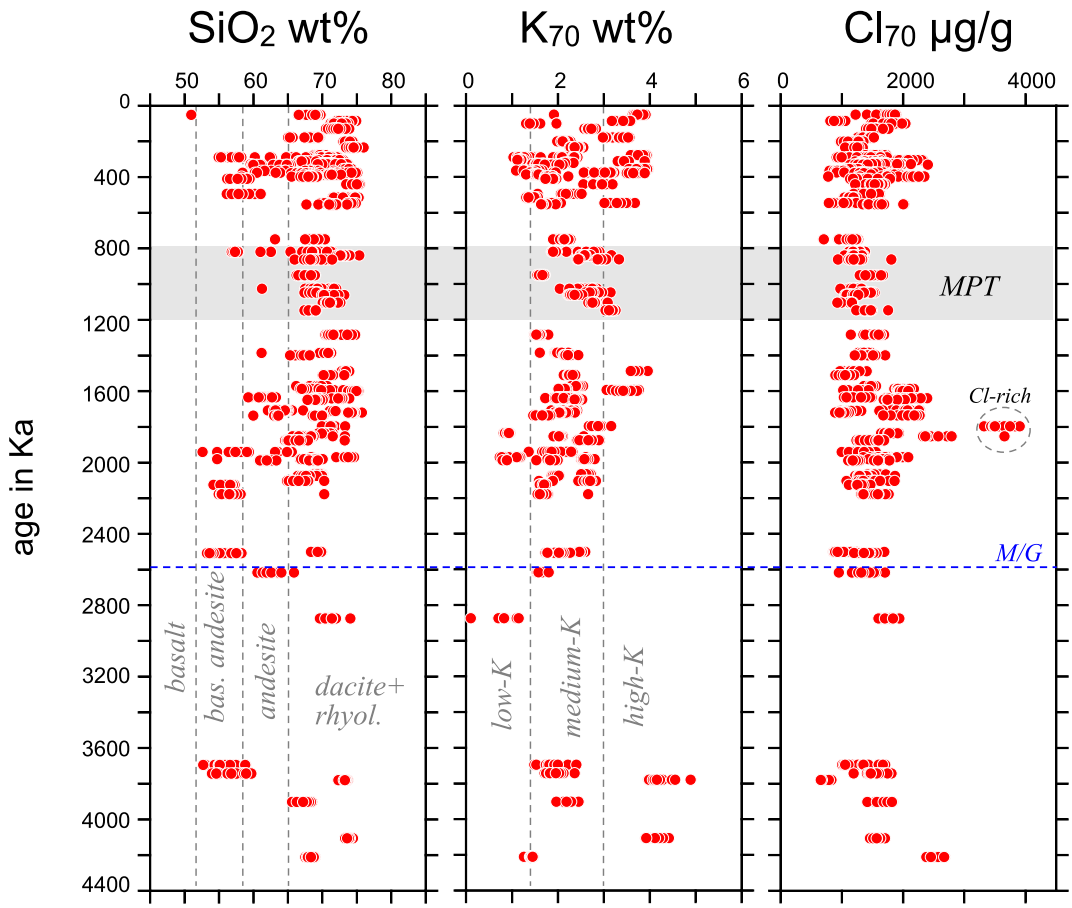

Figure 5. (a) SiO_2 wt%, (b) K_{70} wt%, and (c) Cl_{70} µg/g versus paleomagnetic ages of the 882AB-splice. K_{70} and Cl_{70} are K_2O and Cl wt% normalized to $SiO_2 = 70$ wt%, using equations K_2O wt% = SiO_2 wt% × 0.05–1.75 and Cl µg/g = SiO_2 wt% × 40–1700, in order to highlight their range at a given SiO_2 concentration. MPT—Mid-Pleistocene Transition. M/G—Matuyama/Gauss reversal.

the Nd/La and Nd/Pb ratios are identical to the ratios measured in the onland tephra deposits on Kamchatka (Figure 6) (Portnyagin et al., 2020). No time-progressive trends or shifts are apparent despite some fluctuations. The SiO_2 glass spectrum occasionally widens to include andesitic glasses (e.g., ~400 ka or ~2,000 ka), but there is not co-variation with incompatible elements and element ratios, which pointed to a change in the compositions of the mantle melts. The only outlier of the overall trends is a single, Cl-rich tephra bed (KK110, 882B-9H4-66-73) at 1.8 Myr that is inconspicuous in the major element oxides. This tephra could originate from a Cl-rich eruption from the Kamchatka-Kurile arc, but its provenance remains uncertain due to the lack of trace element or isotope data.

5.4. Increase in Tephra Bed Frequency at the Matuyama-Gauss Reversal

Prueher and Rea (1998) stated that the ash bed frequency increased after a rapid climate change recorded in the subarctic Pacific sediments at the Matuyama-Gauss reversal, where biogenic sediments abruptly transition to glacial-type sediments rich in IRD, dust and ash (Rea et al., 1995). Later, detailed studies of this transition using the 882AB splice confirmed a rapid change to a cooler climate just prior to the Matuyama-Gauss reversal. A fourfold decrease of the biogenic opal accumulation rate at 2.73 Ma coupled with an increase of the Magnetic susceptibility (MS) (Haug et al., 1999, 2005) and the near-doubling of the sedimentary $\delta^{15}N_{bulk}$ (Sigman et al., 2004) were linked to the rapid development of strong subarctic halocline, which was caused by the intensification of the NHG (iNHG) at 2.73 Ma, and the development of extensive ice shields in the Northern hemisphere (Haug et al., 1999; McClymont et al., 2023).

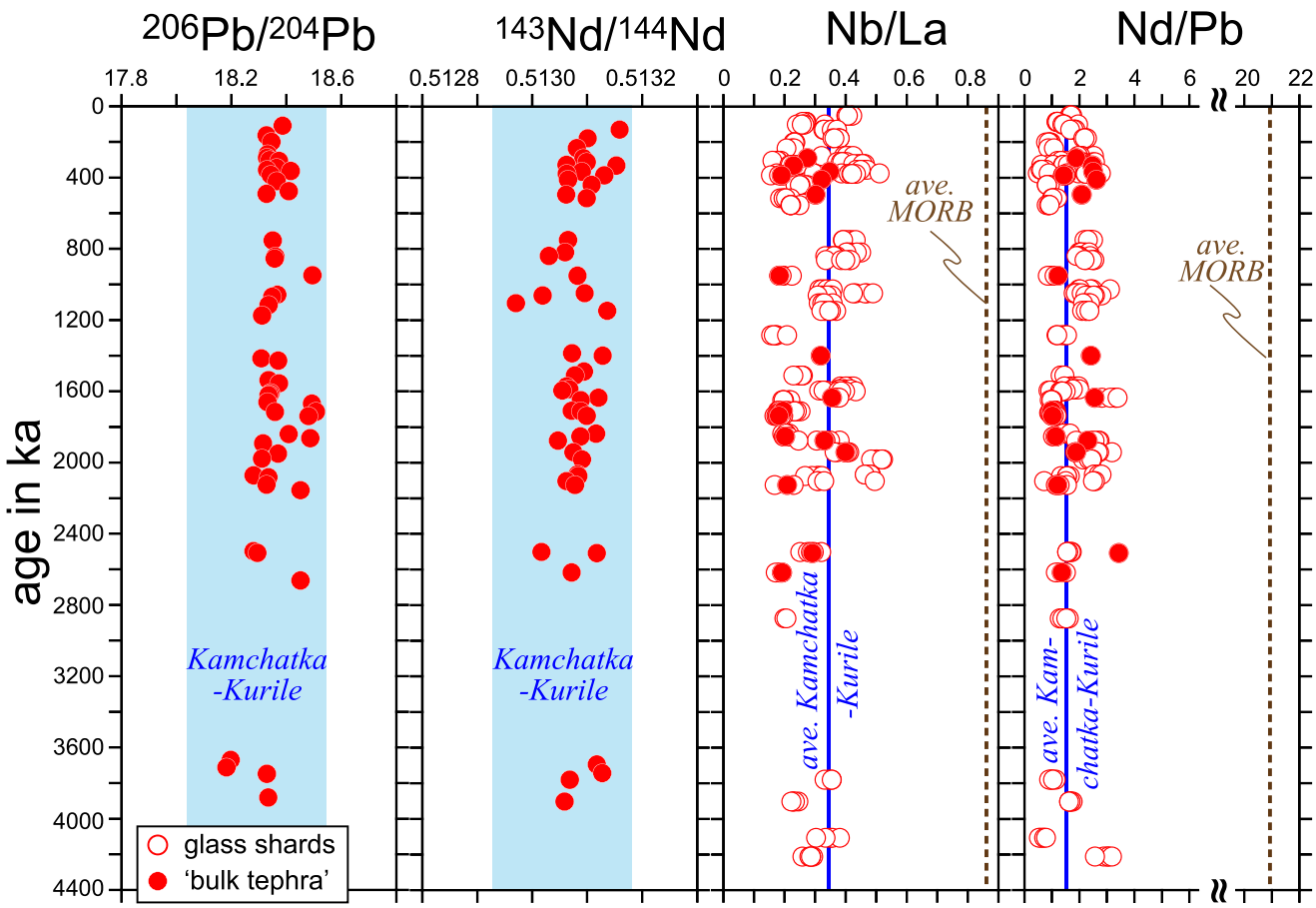

Figure 6. Temporal variations of "bulk tephra" (a) $^{206}Pb/^{204}Pb$, (b) $^{143}Nd/^{144}Nd$, (c) Nb/La, and (d) Nd/Pb versus paleomagnetic ages of 882AB-splice. Kamchatka-Kurile arc range and average for isotope ratios are from Straub (2017); trace element ratios average from subaerial Kamchatka tephra (n = 788 data points) from Portnyagin et al. (2020); average of mid-ocean ridge basalts from Gale et al. (2013).

Because the revised tephrostratigraphies contain only ~1/3 of the ash beds detected by Prueher and Rea (2001), who falsely identified a larger number of ash beds from core photographs, we re-visited the order of events at the Matuyama-Gauss reversal (Figures 7 and 8). The order of events is clear at the most proximal Site 881, located ~770 km east of the Kamchatka-Kurile arc at 2.6 Myr, where the ash bed frequency increases right at 2.6 Myr and follows an incipient increase in the MS—a proxy to IRD but also sensitive to ash and eolian dust (Bailey et al., 2011)—starting earlier the iNHG at 2.73 Ma. The order of events is less clear at Sites 882 and 884, where discrete ash beds are rarer at the respective large paleodistances of ~920 and ~860 km east of the Kamchatka-Kurile arc at 2.6 Ma. Nevertheless, at each site, the MS increases noticeably after (882) or around (884) the iNHG (2.73 Ma) and prior to the appearance of discrete ash beds. The later appearance of the discrete ash beds is tell-tale, because at the large paleodistances they mark very powerful large Kamchatka-Kurile eruptions that occurred just after the iNHG. Thus, the central conclusion of Prueher and Rea (1998) remains that climate change precedes the increase in ash bed frequency, and that therefore climate change must influence volcanism, and not vice versa.

6. Discussion: Establishing a Volcanism-Climate Link

In summary, the information collected for the Site 881–884 ash bed series is straightforward: The ash beds record large-magnitude cataclysmic explosive eruptions (M_v > 5 to 7) of the Kamchatka-Kurile arc. There is no indication from the tephra composition that the Kamchatka-Kurile "volcano-magma systems" —which means the entire magma-producing system from melt-production in the mantle to crustal melt processing prior to explosive eruption—have changed since 4 Ma. All the same, the explosive Kamchatka-Kurile arc volcanism is characterized by alternating cycles of activity and repose, which increase in frequency at the Matuyama-Gauss reversal.

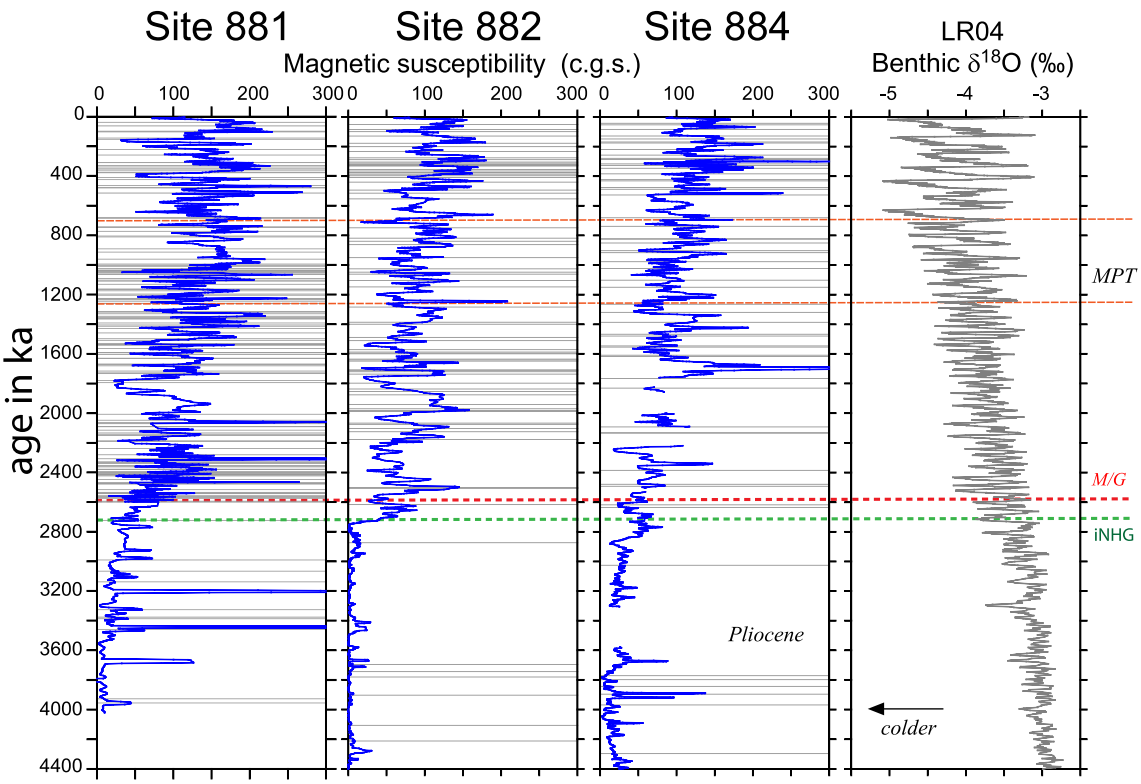

Figure 7. Magnetic susceptibility (MS, blue line) in c.g.s, 10-point running mean of measurements spaced 5 cm apart. Site 881 and 884 MS data from https://web.iodp.tamu.edu/OVERVIEW/?&set=1; Site 882 MS data are from Haug et al. (1999). The MS ages are calculated using the same age models as the tephra bed series. Gray horizontal lines indicate ash beds. MPT—Mid-Pleistocene Transition. M/G—Matuyama/Gauss reversal. iNHG—intensification of Northern hemisphere glaciation. The LR04 benthic $\delta^{18}O$ is from Lisiecki and Raymo (Lisiecki & Raymo, 2005). At the Matuyama-Gauss reversal, the number of ash beds per 1 million years increases from 9 to 53 ash beds at Site 881; from 5 to 28 ash beds in the 882AB-splice; from 4 to 22 ash beds in Hole 882A; and from 5 to 20 at Hole 884B (see also Figure 8).

The question is whether the variations in eruptive frequency could be externally modulated by the co-eval global Plio-Pleistocene climate change, given the coincidence and the sequence of timing between volcanic events and key events of the Plio-Pleistocene climate evolution around the Matuyama-Gauss reversal and the iNGH? In order to test for possible climate links, we compare the ash bed frequency to climate and/or orbital cycles as follows.

6.1. Evidence for Long-Period Trends of Precession and Obliquity Modulation

With only ~13 to 37 ash beds per million years (Table 1), dependencies on the high-frequency Milankovich orbital cycles (precession, obliquity, and eccentricity) cannot be reliably detected at the given age precision of the ODP Site 881–884 tephrostratigraphies (e.g., Zelenin et al., 2024). Moreover, the mere identification of the high-frequency cycles does not provide clear insight into the mechanisms of how the Earth's climate and volcanic systems interact. Instead, the >4 Ma length of the North Pacific records allows us to study processes that operate on hundreds of kyr and longer timescales. At some level, these may be the timescales of greatest interest in these records. While there are no trends in compositional data over this time, tephra layer occurrence and thickness show clear trends indicating long-period variation in arc explosive magnitude.

In order to assess these trends, we performed time series analyses with tephra count and thickness, with the former being a volcanic proxy tracking the relative frequency of all $M_v > \sim 5$ equally, and the latter representing a volcanic proxy effectively weighing for the more robust record of larger-magnitude eruptions in each time window (Figure 9). For our analysis, we use a moving window of 250 kyr to capture sufficient resolution but also be long enough to capture ~6 obliquity (41 kyr) and ~11 precession (19–23 kyr) cycles. Studying these longer timescales also provides robustness to age model uncertainty, as even low-resolution magnetostratigraphic age models are constrained on average, although unevenly spaced in time, by one reversal every 267 kyr over the last 4 Myr. This timescale also provides robustness to slight differences in tephra bed number and thickness among the four Sites 881–884 tephrostratigraphies (Figure 9).

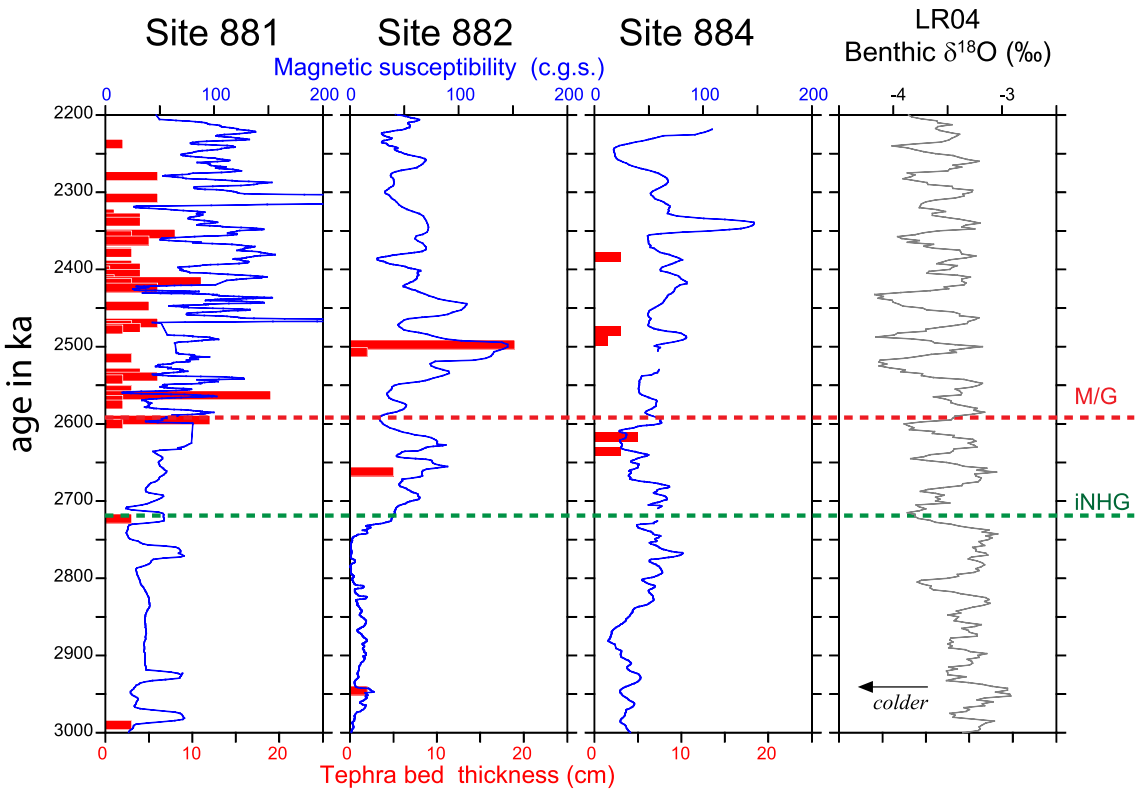

Figure 8. Enlargement of 2.9 to 2.6 Ma, Magnetic susceptibility (MS, blue line) as in Figure 7. M/G—Matuyama/Gauss reversal and iNHG—intensification of Northern hemisphere glaciation. The LR04 benthic $\delta^{18}O$ is from Lisiecki and Raymo (2005).

We compare both the total tephra layer count and the summed tephra thickness in each 250 kyr window in Figure 9. At this scale, the signal is quite robust. In comparing independently counted tephra layers at Site 882 between this study and Ponomareva et al. (2023), we find excellent agreement in the summed tephra thickness. There is good agreement between the total tephra counts in each window. However, our study counts more layers between 1.5 and 2.1 Ma, indicating that we counted more thin layers that do not significantly contribute to the summed tephra thickness. There is also excellent replication of the summed tephra thickness between the three sites for the last 1.8 Ma ("Kamchatka-Kurile Tephra Stack"), indicating the robustness of this proxy to capture regional volcanic changes (Figure 9, right bottom panel).

The records are characterized by times of frequent and thick tephra layers centered at ~0.3, 1.0, and 1.6 Ma and minimal tephra deposition at ~0.6, 1.3, and 1.9 Ma. Before 1.8 Ma, the records are not as coherent, which can be attributed to less continuous recovery (see Site 884 record in Figure 7) or increased distance from the volcanic arc. At this time, the tephra records of the more distal Detroit Sites 882 and 884 (Figures 4–7) become sparse and the record of the more proximal Site 881 may be the most reliable one. Nevertheless, Sites 882 and 881 both show an interval of high summed tephra thickness centered at ~2.5 Ma and Sites 882 and 884 show a period of increased tephra deposition centered at ~3.8 Ma (Figure 9h, right bottom panel).

The timescales associated with the variability in Kamchatka-Kurile explosive volcanism captured by our 250 kyr binned tephra thickness records are similar to the timescales of the amplitude modulation of orbital variations that are important for Pliocene-Pleistocene climate evolution (e.g., the ~400 kyr eccentricity cycle that modulates precession and the ~1.2 Ma amplitude modulation of Earth's obliquity, Figures 10a and 10b, Laskar et al., 2004). The global Earth system response to these orbital variations can be traced using $\delta^{18}O$ measured in benthic foraminifera, which traces global ice volume and deep-sea temperature and displays a clear trend toward larger variability in glacial/interglacial cycles throughout the Plio-Pleistocene (Figures 10c and 10d, Lisiecki & Raymo, 2005; Shackleton, 1967). Much of this increase in variance is thought to have occurred in the absence of direct orbital forcing and can be attributed to the establishment of significant bipolar glaciation during the iNGH

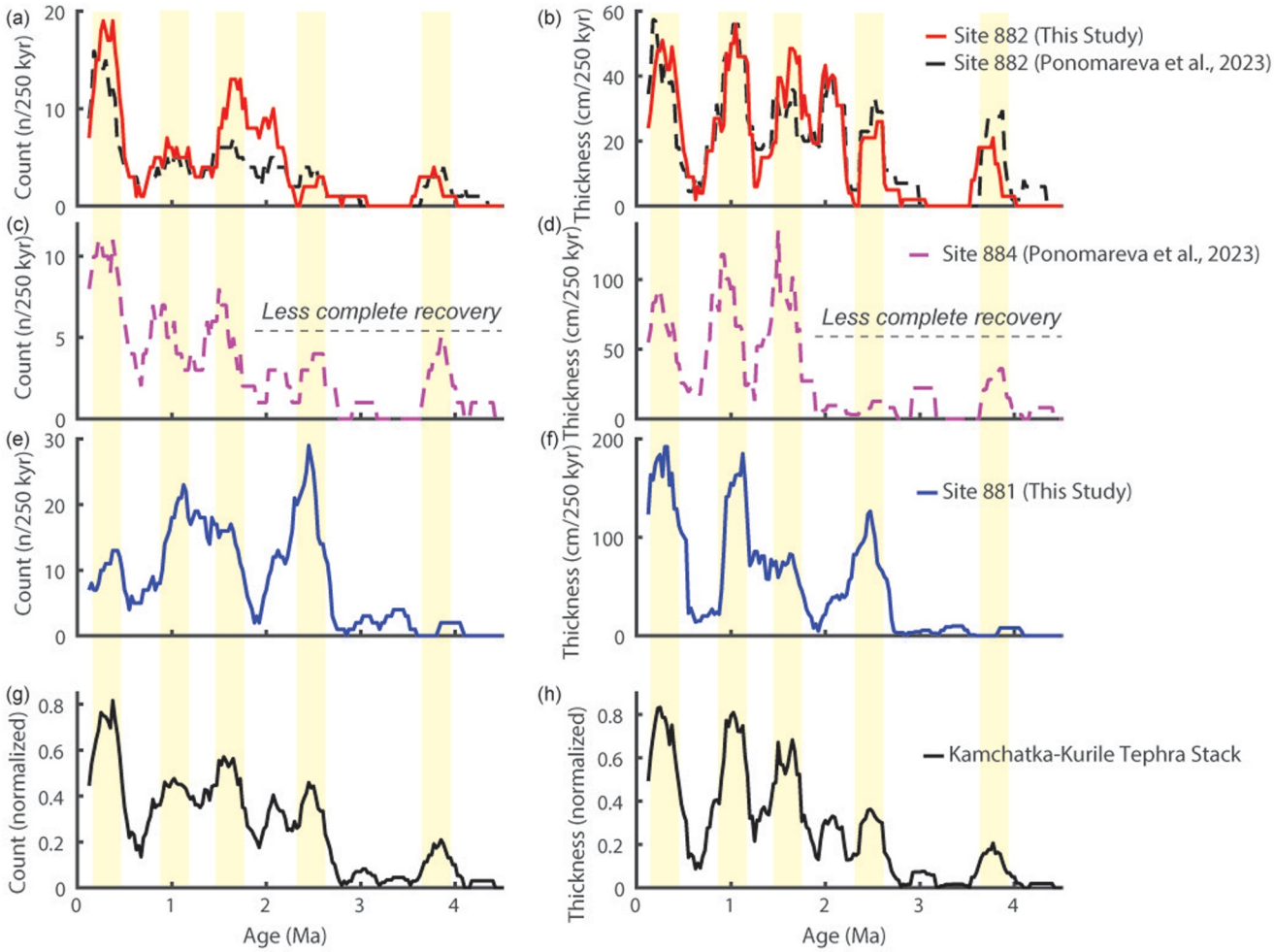

Figure 9. Comparison of Sites 882 (red; dashed black), 884 (dashed magenta), and 881 (blue) total tephra counts (left) and summed tephra thickness (right) per 250 kyr window. Site 882 allows comparison of independently derived tephra records between this study and that of Ponomareva et al. (2023). *Black curve* in the bottom panels is a stacked record to capture the common signal of all three sites. *Yellow shading* indicates time intervals of frequent and high magnitude Kamchatka-Kurile eruptions defined by multiple sites.

and rise of variance at the ~100 kyr eccentricity period during the MPT after ~1.25 Ma (Figures 10d, Clark et al., 2006; Lisiecki & Raymo, 2007).

However, over the last 5 Myr, there is a more proportional response of benthic $\delta^{18}O$ to the amplitude modulation of orbital forcing in the obliquity frequency band (1/38–1/41 kyr^{-1}) prior to the MPT and in the precession frequency band (1/18–1/25 kyr^{-1}) after the MPT [Figures 10e and 10f; analysis after Lisiecki and Raymo (2007) and Reilly et al. (2021); see Text S2 in Supporting Information S1]. Over the last 4 Ma, the highest variability of benthic $\delta^{18}O$ in the precession frequency band occurs at ~0.2 and 1.0 Ma, associated with peaks in the 400 kyr eccentricity cycle that modulate precession at the same time (Figure 10e). The highest variability in benthic $\delta^{18}O$ at in the obliquity frequency band occurred at ~1.4, 2.5, and 3.7 Ma, associated with peak amplitude modulation of Earth's obliquity (Figure 10f). Interestingly, these ages are all within ~100 kyr of where we identified peaks in binned tephra thickness at Sites 882, 884, and 881, occurring at ~0.3, 1.0, 1.6, 2.5, and 3.8 Ma (Figure 9, right bottom panel).

6.2. Simulating the Volcanic Signal With the Components of Variance in Global Ice Volume

To further demonstrate the similarity between North Pacific Kamchatka-Kurile tephra thickness and variability of benthic $\delta^{18}O$ at these timescales, we developed a simple model where variance at the precession and obliquity frequency bands can be used to predict variability in binned tephra thickness over the last 4 Ma. To do so, we

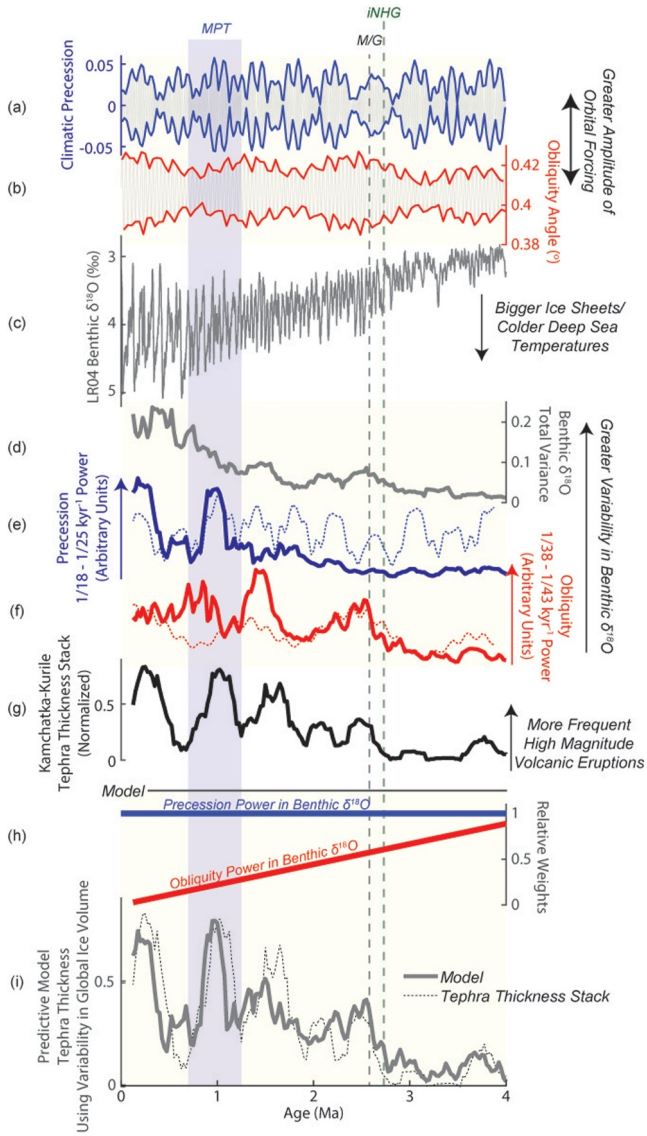

Figure 10. Comparison of the Kamchatka-Kurile tephra thickness record to variability of global ice volume over the last 4 Ma. (a–b) Orbital solutions highlighting the amplitude envelope for climatic precession (blue) and obliquity (red) (Laskar et al., 2004). (c) The LR04 benthic $\delta^{18}O$ stack which tracks the evolution of global ice volume and deep sea temperature (Lisiecki & Raymo, 2005). (d) Total variance of the LR04 stack in a moving 250 kyr window. (e–f) Power in the precession (blue; 1/18–1/25 kyr^{-1}) and obliquity (red; 1/38–1/43 kyr^{-1}) bands for the LR04 stack (solid lines) and orbital solution (dashed lines) in a moving 250 kyr window (g) The Kamchatka-Kurile tephra thickness stack (Figure 9). (h–i) A simple model that uses the time evolution of benthic $\delta^{18}O$ variability at precession and obliquity timescales to explain the time evolution of high magnitude explosive eruptions from the Kamchatka-Kurile volcanic arc. Benthic $\delta^{18}O$ variability at precession timescales dominates the correlation during and after the MPT, while variability at obliquity timescales dominates the correlation prior to the MPT.

develop scaling factors for the power in each frequency band so that variability at the precession timescale is held constant, while the influence at the obliquity timescale becomes less important in the late Pleistocene (Figure 10h). This allows for a rise in variance in the precession band observed in benthic $\delta^{18}O$ (Figure 10e) and decreases the influence of variance at the obliquity timescale after the MPT. This simple model provides an excellent fit to the observations ($r^2 = 0.75$; Figure 10i). Similarly, good fits by this metric can be found by alternative models that keep the scaling between obliquity and precession constant as long as precession is weighted highly enough, as the correlation is largely driven by the precession variation after 1.4 Ma (Text S2 in Supporting Information S1). However, in the latter model, smaller features do not fit as well, such as the smaller Pliocene rise in explosive volcanism around 3.8 Ma.

This correlation provides a direct link between Kamchatka-Kurile arc volcanism and Pliocene-Pleistocene global ice volume, indicating that times with greater frequency and magnitude in volcanic eruptions occurred when there was more significant variability in the amplitude of global ice volume changes at <100 kyr timescales. Because the correlation of these signals occurs on timescales of hundreds of thousands of years, it is robust to orbital scale age model uncertainties that might challenge the phase and frequency analysis of individual tephra layers. Moreover, the origin of the amplitude modulation in global ice volume within the precession and obliquity frequency bands (as traced by benthic $\delta^{18}O$) are well documented to be a direct response to the amplitude modulation of orbital forcing (Lisiecki & Raymo, 2007). We can be confident that climate is the primary control on arc volcanism and not direct orbital forcing itself, as we observe a transition from obliquity to precession at the MPT, which cannot be attributed to direct orbital forcing. As typical for the benthic $\delta^{18}O$ signal of the ice volume changes, the volcanism also increases at 0.2 and 1.0 Ma, but does not increase at the ~0.6 Ma 400 kyr eccentricity cycle peak. Thus, the imprint of this climate signal of the Kamchatka-Kurile tephra record could be considered a "fingerprint" of the mechanism driving this relationship and provides strong support that ice volume, as controlled by changes in Earth's orbit, is a primary driver of the Kamchatka-Kurile arc's Pliocene-Pleistocene evolution and not vice versa. Thus, this "mechanistic fingerprint" is the second indication that volcanism follows climate.

6.3. Linking Glacial Variability and Arc Explosivity: An Outlook

Our study confirms that climate modifies arc volcanicity, and not vice versa. A physical mechanism of how ice volume variability influences volcanism has been outlined by Huybers and Langmuir (2009), who propose that the climate-forced redistribution of ice and water on Earth modulates the melting rate in the mantle. Lower pressure on a given mantle region (e.g., absence of an ice cap on land, or low sea-levels during glacial periods in the ocean) promotes melting, while higher pressure suppresses melt production. Volcanicity may be particularly high at the glacial-interglacial transitions when large stress changes in the Earth's lithosphere facilitated melt ascent. Subsequent studies confirmed that the eruptive activity of single arc volcanoes appears to increase with increased crustal stress, such as because of seawater unloading during glaciation (Satow et al., 2021) or glacial unloading during deglaciation (Rawson et al., 2016).

We propose that changes in the Earth's lithospheric stress field are also responsible for modulating the Kamchatka-Kurile arc volcanism. However, an important difference from previous studies is that the Kamchatka-

Kurile tephra stack does not record the responses to the ice-water redistribution at individual glacial-interglacial transitions. Instead, the tephra patterns recorded longer periods of ∼300 kyr that span several ice cycles (Figure 10) and concurred with the cyclic maxima of the precession and obliquity amplitudes. We proposed that during such maxima the lithospheric stress is augmented, thus promoting larger and more frequent eruptions on top of a "normal" background volcanic signal that may or may not be modulated by the ice cycles.

At first look, the mostly dacitic-rhyolitic composition of the ash beds may suggest that the variability in ice volume triggered melt release from crustal rather than mantle reservoirs. However, it is not possible to thermally sustain silicic crustal reservoirs over several 100 kyrs without adding new heat from recharging mantle melts. The similarity of Pb and Nd isotopes and incompatible element ratios of the mafic and silicic Kamchatka-Kurile melts support a common origin of mafic and evolved magmas from similar mantle sources. Thus, the magmatic flux of the Kurile-Kamchatka volcano-magma systems is ultimately controlled by mantle melting which in turn is modulated by the global variability in ice volume.

A notable feature of the ash bed record is that it has an obliquity variance signal prior to the MPT when obliquity dominates with total global ice volume variability as tracked by benthic $\delta^{18}O$ records. However, following the MPT, the signal of Site 881–884 ash beds is dominated by the eccentricity-modulated precession variance when total global ice volume variability as tracked by benthic $\delta^{18}O$ records is dominated by variability at longer 100-kyr timescales.

We cannot exclude the possibility that a 100 kyr signal may be hidden in the Site 881–884 ash bed record. Currently, only two reliable ash bed records with orbital-scale climate signals exist, which are either from this study or from the IODP Hole 1437B in the oceanic Izu Bonin arc (Schindlbeck, Jegen, et al., 2018). The Hole 1437B record exhibits a solid 100 kyr orbital signal for the last 1.1 Ma, which is carved out by the high count of ash beds per Ma (147 per Myr) that are dated by $\delta^{18}O$ stratigraphy. Due to the high sedimentation rate of 120 m/Myr, many thin ash beds are preserved and contribute to the high count. In contrast, thin ash beds at ODP Sites 881–884 ash beds are rare, presumably having been destroyed by bioturbation at the lower sedimentation rates (35–70 m/Myr). The lower tephra bed count of 13–37 ash beds per Myr, combined with the paleomagnetic method of dating, may simply not allow for resolving a 100 kyr signal in the marine record in contrast to long-period signals (see also, Zelenin et al., 2024).

Alternatively, if the 100-kyr signal is truly absent in the Sites 881–884 ash bed record, other causes are indicated. For example, such absence could be attributed to the sensitivity of the Kamchatka-Kurile volcano-magma systems to the dynamics of the smaller glaciated regions, whereas the larger ice sheets have a larger control on benthic $\delta^{18}O$. Glacial reconstructions over longer timescales indicate repeated Kamchatka-Kurile glaciations through the Pleistocene but with maximum ice extents at different times than the North American and European glacial maximums (Barr & Clark, 2012; Batchelor et al., 2019; Nürnberg et al., 2011). Regional divergence could be due to the sensitivity of regional glaciation to moisture availability influenced by Western European Ice Sheets, and to local insolation forcing (Krinner et al., 2011). Thus, it is possible that regional ice mass changes varied on the shorter obliquity and precession timescales discussed here, and did not experience the 100-kyr ice sheet variability that often characterizes the post-MPT world. Another cause for the missing 100 kyr signal could be a lesser amplitude of pressure change associated with the glacial loading/unloading on the 100 kyr-scale. The Kamchatka-Kurile arc crust, located at some distance from the large North American and Western European ice sheets, may not experience similarly large pressure changes on the crust and peripheral bulge associated with the 100 kyr ice cycles. In this scenario, the Kamchatka-Kurile arc volcano-magma system is less, possibly negligibly, sensitive to the global 100 kyr ice sheet variability, whereas the 100 kyr signal in the oceanic Izu Bonin arc system might have been controlled by the variability of hydrostatic pressure linked to global sea level variations rather than to a regional glacial load.

While such details of time-cause relationships between ice volume variability and solid Earth must await further testing, our study supports the conclusion that arc volcanism can be modulated as a consequence of the establishment of Plio-Pleistocene ice cycles (e.g., Huybers & Langmuir, 2009; Prueher & Rea, 1998). This opens up the possibility that volcanic feedback may help shape the glacial world either by loading the atmosphere with climatically active gases or by increasing the flux of volcaniclastic material to the ocean-atmosphere system. The latter may increase the consumption of CO_2 by increasing oceanic bioproductivity (e.g., Duggen et al., 2010) or by enhanced weathering of the rapidly growing and decaying unstable volcanic terrains.

7. Conclusions

The conclusions of this study are:

- Plio-Pleistocene Kamchatka-Kurile explosive arc volcanism is sensitive to the variability of the global ice volume;
- Maxima in the Kamchatka-Kurile explosive arc volcanism (~0.3, ~1.0, ~1.6, ~2.5, and 3.8 Myr) coincide with maxima of global ice volume variability that have been linked with the amplitude modulation of the precession (0.3, 1.0 Myr) and obliquity (1.6, 2.5, and 3.8 Myr) bands;
- The periodicity of the Kamchatka-Kurile explosive arc volcanism can be reproduced by a model of decreasing obliquity variance across the mid-Pleistocene Transition at constant precession variance, implying its forcing by climate.
- The increase in global ice volume at the iNHG accelerates Kamchatka-Kurile arc volcanism;
- The lack of a direct 100 kyr eccentricity signal in the post MPT ash bed series at Site 881–884 reflects either the comparatively low resolution of the ash bed record at these sites or a possibly regional rather than global influence of ice volume variability.
- Our results support the hypothesis that explosive arc volcanism can respond to global climate variations but not vice versa, except for possible feedbacks.

Conflict of Interest

The authors declare no conflicts of interest relevant to this study.

Data Availability Statement

All Supporting Figure and Tables are uploaded as part of the Supporting Information S1 to this article. All data have been transferred into a FAIR data base (EarthChem) via Straub et al. (2025).

Acknowledgments
Samples and photographs from ODP site 881 and 882 drill cores were provided by the IODP. We thank IODP curator Michelle Penkrot and her staff for their support during sampling at the Gulf coast repository in College Station/TX. Madison Mahan helped with Site 881 data collection. Ofélia Pérez-Arvizu and Liliana Corona are thanked for ICP-MS solution analyses and isotope separation. Fu-Lung Lin assistant with the laser-ablation analyses of the glass shards. Keiji Hammond, Celine Martin and Nick Tailby are thanked for their support with the electron microprobe work. The constructive reviews of Vera Ponomareva and an anonymous reviewer improved the manuscript. This study was financially supported by the U.S. National Science Foundation (Grant OCE-19-50006 to SMS).

References

Bailey, I., Liu, Q., Swann, G. E. A., Jiang, Z., Sun, Y., Zhao, X., & Roberts, A. P. (2011). Iron fertilisation and biogeochemical cycles in the sub-Arctic northwest Pacific during the late Pliocene intensification of northern hemisphere glaciation. *Earth and Planetary Science Letters*, *307*(3), 253–265. https://doi.org/10.1016/j.epsl.2011.05.029

Barr, I. D., & Clark, C. D. (2012). Late Quaternary glaciations in Far NE Russia; combining moraines, topography and chronology to assess regional and global glaciation synchrony. *Quaternary Science Reviews*, *53*, 72–87. https://doi.org/10.1016/j.quascirev.2012.08.004

Barron, J. A., Basov, I. A., Beaufort, L., Dubuisson, G., Gladenkov, A. Y., Morley, J. J., et al. (1995). Biostratigraphic and magnetostratigraphic summary. In D. K. Rea, I. A. Basov, D. W. Scholl, & J. F. Allan (Eds.), *Proceedings of the Ocean Drilling Program Scientific Results Ocean Drilling Program* (pp. 559–575).

Batchelor, C. L., Margold, M., Krapp, M., Murton, D. K., Dalton, A. S., Gibbard, P. L., et al. (2019). The configuration of Northern Hemisphere ice sheets through the Quaternary. *Nature Communications*, *10*(1), 3713. https://doi.org/10.1038/s41467-019-11601-2

Brenna, H., Kutterolf, S., Mills, M. J., & Krüger, K. (2020). The potential impacts of a sulfur- and halogen-rich supereruption such as Los Chocoyos on the atmosphere and climate. *Atmospheric Chemistry and Physics*, *20*(11), 6521–6539. https://doi.org/10.5194/acp-20-6521-202

Bryant, C. J., Arculus, R. J., & Eggins, S. M. (1999). Laser ablation-inductively coupled plasma-mass spectrometry and tephras: A new approach to understanding arc magma genesis. *Geology*, *27*(12), 1119–1122. https://doi.org/10.1130/0091-7613(1999)027<1119:laicpm>2.3.co;2

Bryant, C. J., Arculus, R. J., & Eggins, S. M. (2003). The geochemical evolution of the Izu-Bonin arc system: A perspective from tephras recovered by deep-sea drilling. *Geochemistry, Geophysics, Geosystems*, *4*(11), 1094. https://doi.org/10.1029/2002GC000427

Bubenshchikova, N., Ponomareva, V., Portnyagin, M., Nürnberg, D., Chao, W. S., Lembke-Jene, L., & Tiedemann, R. (2024). The Pauzhetka tephra (South Kamchatka): A key middle Pleistocene isochron for the Northwest Pacific and Okhotsk Sea sediments. *Quaternary Geochronology*, *79*, 101476. https://doi.org/10.1016/j.quageo.2023.101476

Cambray, H., Cadet, J. P., & Pouclet, A. (1993). Ash layers in deep-sea sediments as tracers of arc volcanic activity: Japan and Central America as case studies. *The Island Arc*, *2*, 72–86. https://doi.org/10.1111/j.1440-1738.1993.tb00075.x

Cao, L. Q., Arculus, R. J., & McKelvey, B. C. (1995). Geochemistry and petrology of volcanic ashes recovered from sites 881 through 884: A temporail record of Kamchatka and Kurile volcanism. In D. K. Rea, I. A. Basov, D. W. Scholl, & J. F. Allan (Eds.), *Proceedings of the Ocean Drilling Program Scientific Results Ocean Drilling Program* (pp. 345–381).

Clark, P. U., Archer, D., Pollard, D., Blum, J. D., Rial, J. A., Brovkin, V., et al. (2006). The middle Pleistocene transition: Characteristics, mechanisms, and implications for long-term changes in atmospheric pCO_2. *Quaternary Science Reviews*, *25*(23), 3150–3184. https://doi.org/10.1016/j.quascirev.2006.07.008

Crosweller, H. S., Arora, B., Brown, S. K., Cottrell, E., Deligne, N. I., Ortiz Guerrero, N., et al. (2012). Global database on large magnitude explosive volcanic eruptions (LaMEVE). *Journal of Applied Volcanology*, *1*, 4. https://doi.org/10.1186/2191-5040-1-4

Deligne, N. I., Coles, S. G., & Sparks, R. S. J. (2010). Recurrence rates of large explosive volcanic eruptions. *Journal of Geophysical Research*, *115*(B6), B06203. https://doi.org/10.1029/2009JB006554

Duggen, S., Olgun, N., Croot, P., Hoffmann, L., Dietze, H., Delmelle, P., & Teschner, C. (2010). The role of airborne volcanic ash for the surface ocean biogeochemical iron-cycle: A review. *Biogeosciences*, *7*(3), 827–844. https://doi.org/10.5194/bg-7-827-2010

Dupre, B., & Allegre, C. (1983). Pb-Sr isotopic variations in Indian Ocean basalts and mixing phenomena. *Nature*, *286*, 142–146. https://doi.org/10.1038/303142a0

Freundt, A., Schindlbeck-Belo, J. C., Kutterolf, S., & Hopkins, J. L. (2021). Tephra layers in the marine environment: A review of properties and emplacement processes. *Geological Society, London, Special Publications*, *520*(1), 595–637. https://doi.org/10.1144/sp520-2021-50

Gale, A., Dalton, C. A., Langmuir, C. H., Su, Y., & Schilling, J. G. (2013). The mean composition of ocean ridge basalts. *Geochemistry, Geophysics, Geosystems*, *14*(3), 489–518. https://doi.org/10.1002/ggge.20038

Haug, G. H., Ganopolski, A., Sigman, D. M., Rosell-Mele, A., Swann, G. E. A., Tiedemann, R., et al. (2005). North Pacific seasonality and the glaciation of North America 2.7 million years ago. *Nature*, *433*(7028), 821–825. https://doi.org/10.1038/nature03332

Haug, G. H., Sigman, D. M., Tiedemann, R., Pedersen, T. P., & Sarnthein, M. (1999). Onset of permanent stratification in the subarctic Pacific Ocean. *Nature*, *401*(6755), 779–782. https://doi.org/10.1038/44550

Huybers, P., & Langmuir, C. H. (2009). Feedback between deglaciation, volcanism, and atmospheric CO_2. *Earth and Planetary Science Letters*, *286*(3–4), 479–491. https://doi.org/10.1016/j.epsl.2009.07.014

Kennett, J. P., & Thunell, R. C. (1977). On explosive cenozoic volcanism and climatic implications. *Science*, *196*(4295), 1231–1234. https://doi.org/10.1126/science.196.4295.1231-a

Krinner, G., Diekmann, B., Colleoni, F., & Stauch, G. (2011). Global, regional and local scale factors determining glaciation extent in Eastern Siberia over the last 140,000 years. *Quaternary Science Reviews*, *30*(7), 821–831. https://doi.org/10.1016/j.quascirev.2011.01.001

Kutterolf, S., Jegen, M., Mitrovica, J. X., Kwasnitschka, T., Freundt, A., & Huybers, P. J. (2013). A detection of Milankovitch frequencies in global volcanic activity. *Geology*, *41*(2), 227–230. https://doi.org/10.1130/G33419.1

Kutterolf, S., Schindlbeck, J. C., Jegen, M., Freundt, A., & Straub, S. M. (2019). Milankovitch frequencies in tephra records at volcanic arcs: The relation of kyr-scale cyclic variations in volcanism to global climate changes. *Quaternary Science Reviews*, *204*, 1–16. https://doi.org/10.1016/j.quascirev.2018.11.004

Kutterolf, S., Schindlbeck, J. C., Robertson, A. H. F., Avery, A., Baxter, A. T., Petronotis, K., & Wang, K. L. (2018). Tephrostratigraphy and provenance from IODP Expedition 352, Izu-Bonin arc: Tracing tephra sources and volumes from the Oligocene to recent. *Geochemistry, Geophysics, Geosystems*, *19*(1), 150–174. https://doi.org/10.1002/2017GC007100

Laskar, J., Robutel, P., Joutel, F., Gastineau, M., Correia, A. C. M., & Levrard, B. (2004). A long-term numerical solution for the insolation quantities of the Earth. *Astronomy & Astrophysics*, *428*(1), 261–285. https://doi.org/10.1051/0004-6361:20041335

Legros, F. (2000). Minimum volume of a tephra fallout deposit estimated from a single isopach. *Journal of Volcanology and Geothermal Research*, *96*(1), 25–32. https://doi.org/10.1016/s0377-0273(99)00135-3

Lisiecki, L. E., & Raymo, M. E. (2005). A Pliocene-Pleistocene stack of 57 globally distributed $\delta^{18}O$ records. *Palaeoceanography*, *20*(1), PA1003. https://doi.org/10.1029/2004PA001071

Lisiecki, L. E., & Raymo, M. E. (2007). Plio–Pleistocene climate evolution: Trends and transitions in glacial cycle dynamics. *Quaternary Science Reviews*, *26*(1), 56–69. https://doi.org/10.1016/j.quascirev.2006.09.005

Longman, J., Gernon, T., Hincks, T., Panitz, S., & Palmer, M. (2024). Intensified global volcanism during Late Pleistocene glacial strength shift. *Nature Portfolio*. PREPRINT. https://doi.org/10.21203/rs.3.rs-3954094/v1

Mahony, S. H., Barnard, N. H., Sparks, R. S. J., & Rougier, J. C. (2020). VOLCORE, a global database of visible tephra layers sampled by ocean drilling. *Scientific Data*, *7*(1), 330. https://doi.org/10.1038/s41597-020-00673-1

Mahony, S. H., Sparks, R. S. J., Wallace, L. M., Engwell, S. L., Scourse, E. M., Barnard, N. H., et al. (2016). Increased rates of large-magnitude explosive eruptions in Japan in the late Neogene and Quaternary. *Geochemistry, Geophysics, Geosystems*, *17*(7), 2467–2479. https://doi.org/10.1002/2016GC006362

Mason, B. G., Pyle, D. M., & Oppenheimer, C. (2004). The size and frequency of the largest explosive eruptions on Earth. *Bulletin of Volcanology*, *66*(8), 735–748. https://doi.org/10.1007/s00445-004-0355-9

McClymont, E. L., Ho, S. L., Ford, H. L., Bailey, I., Berke, M. A., Bolton, C. T., et al. (2023). Climate evolution through the onset and intensification of Northern Hemisphere glaciation. *Reviews of Geophysics*, *61*(3), e2022RG000793. https://doi.org/10.1029/2022rg000793

Nürnberg, D., Dethleff, D., Tiedemann, R., Kaiser, A., & Gorbarenko, S. A. (2011). Okhotsk Sea ice coverage and Kamchatka glaciation over the last 350 ka — Evidence from ice-rafted debris and planktonic $\delta^{18}O$. *Palaeogeography, Palaeoclimatology, Palaeoecology*, *310*(3), 191–205. https://doi.org/10.1016/j.palaeo.2011.07.011

Pank, K., Kutterolf, S., Schindlbeck-Belo, J. C., Hopkins, J. L., Wang, K. L., Lee, H. Y., & Schmitt, A. K. (2023). Advances in New Zealand's tephrochronostratigraphy - A continuous 12 Ma eruption record based on marine tephra from deep ocean drilling east of New Zealand. In *AGU Fall Meeting, San Francisco* (pp. V13D–V0160).

Paterne, M., Guichard, F., & Labeyrie, J. (1988). Explosive activity of the South Italian volcanoes during the past 80,000 Years as determined by marine tephrochronology. *Journal of Volcanology and Geothermal Research*, *34*(3–4), 153–172. https://doi.org/10.1016/0377-0273(88)90030-3

Ponomareva, V., Bubenshchikova, N., Portnyagin, M., Zelenin, E., Derkachev, A., Gorbarenko, S., et al. (2018). Large-magnitude Pauzhetka caldera-forming eruption in Kamchatka: Astrochronologic age, composition and tephra dispersal. *Journal of Volcanology and Geothermal Research*, *366*, 1–12. https://doi.org/10.1016/j.jvolgeores.2018.10.006

Ponomareva, V. V., Portnyagin, M. V., Bubenshchikova, N. V., Zelenin, E. A., Derkachev, A. N., Jicha, B., et al. (2023). A 6.2 Ma-long record of major explosive eruptions from the NW Pacific volcanic arcs based on the offshore tephra sequences on the northern tip of the Emperor Seamount Chain. *Geochemistry, Geophysics, Geosystems*, *24*(12), e2023GC011126. https://doi.org/10.1029/2023gc011126

Portnyagin, M. V., Ponomareva, V. V., Zelenin, E. A., Bazanova, L. I., Pevzner, M. M., Plechova, A. A., et al. (2020). TephraKam: Geochemical database of glass compositions in tephra and welded tuffs from the Kamchatka volcanic arc (northwestern Pacific). *Earth System Science Data*, *12*(1), 469–486. https://doi.org/10.5194/essd-12-469-2020

Prueher, L. M., & Rea, D. K. (1998). Rapid onset of glacial conditions in the subarctic North Pacific region at 2.67 Ma: Clues to causality. *Geology*, *26*(11), 1027–1030. https://doi.org/10.1130/0091-7613(1998)026<1027:roogci>2.3.co;2

Prueher, L. M., & Rea, D. K. (2001). Tephrochronology of the Kamchatka-Kurile and Aleutian arcs: Evidence for volcanic episodicity. *Journal of Volcanology and Geothermal Research*, *106*(1–2), 67–84. https://doi.org/10.1016/s0377-0273(00)00266-3

Pyle, D. M. (1995). Mass and energy budgets of explosive volcanic eruptions. *Geophysical Research Letters*, *22*(5), 563–566. https://doi.org/10.1029/95gl00052

Rawson, H., Pyle, D. M., Mather, T. A., Smith, V. C., Fontijn, K., Lachowycz, S. M., & Naranjo, J. A. (2016). The magmatic and eruptive response of arc volcanoes to deglaciation: Insights from southern Chile. *Geology*, *44*(4), 252–254. https://doi.org/10.1130/G37504.1

Rea, D. K., Basov, I. A., Janecek, T. R., & Palmer-Julson, A. (1993). *Proceedings of the Ocean Drilling Program, Initial Reports* (Vol. 145, pp. 37–83).

Rea, D. K., Basov, I. A., Krissek, L. A., & Leg 145 Scientific Party. (1995). Scientific results of drilling the North Pacific Transect. In *Proceedings of the Ocean Drilling Program, Scientific Results* (Vol. 145, pp. 577–596).

Reilly, B. T., Tauxe, L., Brachfeld, S., Raymo, M., Bailey, I., Hemming, S., et al. (2021). New magnetostratigraphic insights from Iceberg Alley on the rhythms of Antarctic climate during the Plio-Pleistocene. *Paleoceanography and Paleoclimatology*, *36*(2), e2020PA003994. https://doi.org/10.1029/2020pa003994

Satow, C., Gudmundsson, A., Gertisser, R., Ramsey, C. B., Bazargan, M., Pyle, D. M., et al. (2021). Eruptive activity of the Santorini Volcano controlled by sea-level rise and fall. *Nature Geoscience*, *14*(8), 586–592. https://doi.org/10.1038/s41561-021-00783-4

Schindlbeck, J. C., Jegen, M., Freundt, A., Kutterolf, S., Straub, S. M., Mleneck-Vautravers, M. J., & McManus, J. (2018). 100- kyr cyclicity in volcanic ash emplacement: Evidence from a 1.1 Myr tephra record from the NW Pacific. *Scientific Reports*, *8*(1), 4440. https://doi.org/10.1038/s41598-018-22595-0

Schindlbeck, J. C., Kutterolf, S., Straub, S. M., Andrews, G. D. M., Wang, K. L., & Mleneck-Vautravers, M. J. (2018). The 1 Ma - Recent Tephra Record at IODP Sites U1436 and U1437: Insights into explosive volcanism from the Japan and Izu arcs. *The Island Arc*, *27*(3), e12244. https://doi.org/10.1111/iar.12244

Shackleton, N. (1967). Oxygen isotope analyses and Pleistocene temperatures re-assessed. *Nature*, *215*(5096), 15–17. https://doi.org/10.1038/215015a0

Sigman, D., Jaccard, S., & Haug, G. (2004). Polar ocean stratification in a cold climate. *Nature*, *428*(6978), 59–63. https://doi.org/10.1038/nature02357

Straub, S. M. (2003). The evolution of the Izu Bonin - Mariana volcanic arcs (NW Pacific) in terms of major elements. *Geochemistry, Geophysics, Geosystems*, *4*(2), 1018. https://doi.org/10.1029/2002GC000357

Straub, S. M. (2017). Compilation of published major and trace elements and Sr-Nd-Pb-Hf isotope ratios of Quaternary-age arc volcanic rocks from 9 arc settings. *EarthChem Library*. https://doi.org/10.1594/IEDA/100664

Straub, S. M., Reilly, B., Raymo, M. E., Gómez-Tuena, A., Wang, K., Widom, E., et al. (2025). Major and trace element data of volcanic glass shards from ash beds drilled at ODP Site 882; trace element and Pb-Nd isotope analyses of separated fresh volcanic particles from ODP Site 882 ash beds, Version 1.0. *Interdisciplinary Earth Data Alliance (IEDA)*. https://doi.org/10.60520/IEDA/113223

Straub, S. M., & Schmincke, H. U. (1998). Evaluating the tephra input into Pacific Ocean sediments: Distribution in time and space. *International Journal of Earth Sciences*, *87*(3), 461–476. https://doi.org/10.1007/s005310050222

Straub, S. M., Woodhead, J. D., & Arculus, R. J. (2015). Temporal evolution of the Mariana Arc: Mantle wedge and subducted slab controls revealed with a tephra perspective. *Journal of Petrology*, *56*, 2–439. https://doi.org/10.1093/petrology/egv005

Tiedemann, R., & Haug, G. H. (1995). Astronomical calibration of cycle stratigraphy for Site 882 in the northwest Pacific. In D. K. Rea, I. A. Basov, D. W. Scholl, & J. F. Allan (Eds.), *Proceedings of the Ocean Drilling Program Scientific Results* (pp. 283–292).

Weeks, R. J., Roberts, A. P., Verosub, K. L., Okada, M., & Dubuisson, G. J. (Eds.). (1995). *Magnetostratigraphy of upper Cenozoic sediments from leg 145, North Pacific Ocean. Proceedings of the Ocean Drilling Program Scientific results* (Vol. 145, pp. 491–521). Texas A & M University, Ocean Drilling Program.

Zelenin, E., Garipova, S., Ponomareva, V., Portnyagin, M., & Dolgaya, A. (2024). Temporal characteristics of a 6.2 Ma-long ash-fall history in the NW Pacific. *Journal of Volcanology and Geothermal Research*, *453*, 108141. https://doi.org/10.1016/j.jvolgeores.2024.108141

References From the Supporting Information

Devine, J. D., Gardener, J. E., Brack, H. P., Layne, G. D., & Rutherford, M. J. (1995). Comparison of microanalytical methods for estimating H_2O contents of silicic volcanic glasses. *American Mineralogist*, *80*, 319–328.

Garçon, M., Boyet, M., Carlson, R. W., Horan, M. F., Auclair, D., & Mock, T. D. (2018). Factors influencing the precision and accuracy of Nd isotope measurements by thermal ionization mass spectrometry. *Chemical Geology*, *476*, 493–514. https://doi.org/10.1016/j.chemgeo.2017.12.003

GeoREM. (2023). Database on geological and environmental reference material. Retrieved from http://georem.mpch-mainz.gwdg.de/

Gómez-Tuena, A., LaGatta, A., Langmuir, C. H., Goldstein, S. L., Ortega-Gutiérrez, F., & Carrasco-Nunez, G. (2003). Temporal control of subduction magmatism in the eastern Trans-Mexican Volcanic Belt: Mantle sources, slab contributions, and crustal contamination. *Geochemistry, Geophysics, Geosystems*, *8*(4), 8913. https://doi.org/10.1029/2002GC000421

Gómez-Tuena, A., Laura Mori, L., Goldstein, S. L., & Perez-Arvizu, O. (2011). Magmatic diversity of western Mexico as a function of metamorphic transformations in the subducted oceanic plate. *Geochimica et Cosmochimica Acta*, *75*(1), 213–241. https://doi.org/10.1016/j.gca.2010.09.029

Hamilton, T. S. (1995). Seismic stratigraphy of Cenozoic sediments from North Pacific Seamount Platform and Deep-Sea Sites, Leg 145. In D. K. Rea, I. A. Basov, D. W. Scholl, & J. F. Allan (Eds.), *Proceedings of the Ocean Drilling Program, Scientific Results* (Vol. 145, pp. 437–453). Ocean Drilling Program. https://doi.org/10.2973/odp.proc.sr.145.136.1995

Jarosewich, E., Nelen, N., & Norberg, J. (1980). Reference samples for electron microprobe analysis. *Geostandards Newsletter*, *4*(1), 43–47. https://doi.org/10.1111/j.1751-908x.1980.tb00273.x

Jochum, K. P., Stoll, B., Herwig, K., Willbold, M., Hofmann, A. W., Amini, M., et al. (2006). MPI-DING reference glasses for in situ microanalysis: New reference values for element concentrations and isotope ratios. *Geochemistry, Geophysics, Geosystems*, *7*(2), Q02008. https://doi.org/10.1029/2005gc001060

Jweda, J., Bolge, L., Class, C., & Goldstein, S. L. (2016). High precision Sr-Nd-Hf-Pb isotopic compositions of USGS Reference Material BCR-2. *Geostandards and Geoanalytical Research*, *40*(1), 101–115. https://doi.org/10.1111/j.1751-908x.2015.00342.x

Kamenov, G. D., Mueller, P. A., & Perfit, M. R. (2004). Optimization of mixed Pb/Tl solutions for high precision isotopic analyses by MC-ICP-MS. *Journal of Analytical Atomic Spectrometry*, *19*(9), 1262–1267. https://doi.org/10.1039/b403222e

Morgan, G. B., & London, D. (1996). Optimizing the electron microprobe analysis of hydrous alkali aluminosilicate glasses. *American Mineralogist*, *81*(9–10), 1176–1185. https://doi.org/10.2138/am-1996-9-1016

Mori, L., Gómez-Tuena, A., Cai, Y. M., & Goldstein, S. L. (2007). Effects of prolonged flat subduction on the Miocene magmatic record of the central Trans-Mexican Volcanic Belt. *Chemical Geology*, *244*(3–4), 452–473. https://doi.org/10.1016/j.chemgeo.2007.07.002

Newhall, C. G., & Self, S. (1982). The volcanic explosivity index (VEI) an estimate of explosive magnitude for historical volcanism. *Journal of Geophysical Research*, *87*(C2), 1231–1238.

Todt, W., Cliff, R. A., Hanser, A., & Hofmann, A. W. (1996). Evaluation of a 202Pb-205Pb double-spike for high-precision lead isotope analysis. In A. Basu & S. R. Hart (Eds.), *Earth Processes: Reading the Isotopic Code* (pp. 429–437). AGU. https://doi.org/10.1029/GM095p0429

van Achterberg, E., Ryan, C., Jackson, S., & Griffin, W. (2001). LA-ICP-MS in the Earth Sciences - Appendix 3, data reduction software for LA-ICP-MS. *Short Course*, *29*, 239–243.